Influence of stoichiometry and structure on the optical properties of AlN_xO_y films

J Borges[1], N P Barradas[2], E Alves[2], M F Beaufort[3], D Eyidi[3], F Vaz[1] and L Marques[1]

[1]Centro/Departamento de Física, Universidade do Minho, 4710-057 Braga, Portugal

[2]Instituto Superior Técnico/ITN, Universidade Técnica de Lisboa, E.N. 10, 2686-953 Sacavém, Portugal

[3]Institut Pprime - UPR 3346 CNRS-Université de Poitiers-ENSMA, Département de Physique et Mécanique des Matériaux Bât. SP2MI - Téléport 2, BP 30179 F86962 Futuroscope Chasseneuil Cedex, France

E-mail: joelborges@fisica.uminho.pt

Abstract. The AlN_xO_y system offers the possibility to obtain a wide range of responses, by tailoring the properties between Al, AlN and Al_2O_3, opening a significant number of possible applications. The aim of this work is to correlate the optical properties of AlN_xO_y thin films with their composition and structural features, taking as reference the binary systems AlN_x and AlO_y. In the AlN_x system, the increase of the nitrogen content induced a wide variation in the optical properties, ranging from the typical profile of a polycrystalline Al-type film towards nearly constant reflectance values as low as 5%, as well as a smooth increase in samples transparency as the ratio N/Al approached unit. In the case of the AlO_y system, the reflectance also decreased as the oxygen content increased, however the transition to transparent films (Al_2O_3-like) was more abrupt. The ternary system AlN_xO_y, revealed optical responses that ranged from a typical profile of a polycrystalline Al-type film, towards low and constant reflectance values in a wide range of x and y coefficients, ending up as semi-transparent when Al_2O_3-like films were formed. The unusual low optical reflectance of some films reveals some potential applications in solar power systems and sensors.

Keywords: AlN_xO_y, magnetron sputtering, stoichiometry, structure, optical properties.

1. INTRODUCTION

Metallic oxynitride thin films, MeN_xO_y (with Me standing for a metal), are a class of materials that are attracting the attention of several researchers for the last decade due to their interesting properties in different technological domains such as protective applications [1], decorative coatings for high-quality consumer products [2, 3], gas barriers [4], optoelectronics [5] microelectronics [6], solar cells [7], among others. In fact, it has been shown that by varying the non-metallic over metallic content in the films, it is possible to obtain a large gradient of different properties [2, 5, 8-23], including the optical ones, which are always of high interest. Martin *et al.* [24], Vaz *et al.* [2], Chappé *et al.* [9] and Venkataraj *et al.* [11] studied the TiN_xO_y system and found that the colour of the films [2, 9], the optical constants (refractive index, n and extinction coefficient, k) [11], as well as the bandgap [10] can be tuned according to the non-metallic/Ti atomic ratios. Carvalho *et al.* [20] claimed that distinct intrinsic colours can also be found in the ZrN_xO_y system, according to the concentration of non-metallic elements in the films. In other related works, Banakh *et al.* [16], Mientus *et al.* [15], Parreira *et al.* [17], Futsuhara *et al.* [8], Fenker *et al.* [21], Petitjean *et al.* [23] and Venkataraj *et al.* [11] also showed that by controlling the oxygen-to-nitrogen ratio, respectively, in TaN_xO_y, CrN_xO_y, WN_xO_y, ZnN_xO_y, NbN_xO_y, FeN_xO_y and HfN_xO_y systems, they were able to tune properties such as the bandgap and the crystallographic structure between nitride and oxide, and hence the overall optical properties. All these works support the idea that the optical properties of the metallic oxynitrides can be tailored from the pure metal towards the pure metallic oxide and nitride binary systems, according to the particular application envisaged.

Among the possible metallic oxynitrides, aluminium oxynitride (AlN_xO_y) is also another attractive system to be studied in terms of optical properties, since one can find a wide range of properties in this ternary system. This possibility arises from the particular characteristics of each base system, since aluminium is a metallic material; while aluminium nitride (AlN) is a semiconductor with a bandgap in the range of 5.8 to 6.2 eV [25], and a refractive index varying between 1.8 – 2.2 [26-28]; and aluminium oxide (Al_2O_3), is a well-known and used insulator, with a bandgap as high as 9 eV and a low refractive index in the order of 1.7 – 1.8 in the visible range [26, 29-31]. In fact, Al, AlN and Al_2O_3 are used in several different technological fields and applied in a large variety of different devices. First of all, aluminium is used in mirror fabrication, as well as in surface plasmon-coupled emission (SPCE) applications, and it is a good candidate to be used as non-resonant plasmonic nanoparticle in thin-film silicon solar cells [32-34]. Due to its semiconductor characteristics, AlN is commonly used in fabrication of optical sensors in the ultraviolet-visible region, light emitting diodes (LEDs) [35], and several types of microelectronic-related applications [36-39]. Finally, alumina, Al_2O_3, is used as protective film for metal reflectors, dark mirrors, and in metal-oxide-semiconductor devices [40].

The possibility to tailor the properties of aluminium oxynitride thin films between those of pure aluminium and those of aluminium oxide and nitride films, or to combine some of their advantages by varying the elemental concentrations, allows developing a mixed Al-N-O system, where the optical properties can be tuned according to the required application. There are some studies related with the polycrystalline spinel aluminium oxynitride which is known to be a ceramic material (melting point above 2300 K) with high strength and hardness [41], and it has a refractive index between 1.6 and 1.8, being transparent between 230 and 5000 nm [26]. Spinel- AlNO is claimed to develop a face centered cubic lattice, when stabilized at very high temperature in a nitrogen atmosphere [42], exhibiting a lattice parameter of approximately 0.79 nm. This cubic symmetry ensures isotropic optical properties for the polycrystalline AlNO, which implies a reduction of the optical scattering. This set of features has allowed aluminium oxynitride to be considered, for example, a candidate for the American armour systems [43], since it offers advantages when compared with glass and sapphire (Al_2O_3). AlNO has also been claimed to be a high reliability coating for the improvement of the catastrophic optical damage of LASER diodes [44], and it is used in upconversion luminescence materials [45]. Finally, AlNO thin films can also be used in solar collectors and concentrated solar power systems, due to their relatively high solar absorbance [46].

Taking the above as a starting point, this work is devoted to study the influence of stoichiometry and structure in the optical responses of AlN_xO_y thin films and comparing these responses with those of the two base binary systems: AlN_x and AlO_y. Since the optical properties of the materials significantly depend on their interdependence of composition and type of bonding, structure, and morphology, an understanding of these relationships will be a major concern. In this respect, this work can be considered as a contribution to the understanding of a class of materials whose interest is growing in the past few years: the oxynitrides. This basic knowledge on oxynitrides (aluminium oxynitride in the present case) is fundamental to establish the limits for practical applicability of these coatings in future applications where the major findings of this work might be of importance.

2. EXPERIMENTAL DETAILS

For the present work, AlN_x, AlO_y and AlN_xO_y films were deposited on glass and <100> silicon substrates by reactive DC magnetron sputtering, in a homemade deposition system [12, 13, 47]. The substrates were ultrasonically cleaned and then placed in the rotating substrate holder. They were grounded and heated before discharge ignition by using a heating resistor placed at 80 mm from its surface, controlled by a type-K thermocouple. When the base pressure was close to ~10^{-4} Pa the substrates were subjected to an *in situ* etching process, using pure argon with a partial pressure of ~

0.3 Pa, and a pulsed DC current of 0.6 A for 900 s. The films were prepared with the power supply connected to the magnetron operating in the current regulating mode by applying a direct current (DC) density on the aluminium target. The gas atmosphere was composed of argon and a reactive gas composed of a nitrogen + oxygen mixture, with a N_2 + O_2 constant ratio of 17:3, in order to prepare the oxynitride films, AlN_xO_y. In the case of the binary systems, the argon was mixed up with pure N_2 and pure O_2 in order to produce AlN_x and AlO_y films, respectively. The partial pressure of reactive gas was measured just before discharge ignition, without argon, and keeping constant the other deposition parameters (temperature, ground condition and base pressure), and thus it is directly proportional to the gas flow rate. In order to remove oxide/nitride layers from the cathode surface before each deposition without substrates in the chamber, a cleaning of the target was performed by applying the same current density and argon pressure, until the target potential was constant. Further details of the experimental setup can be found elsewhere [12, 47]. Table 1 summarizes the sputtering conditions/parameters used to produce the three sets of films of AlN_x, AlO_y and AlN_xO_y.

Sputtering conditions/parameters	**Value**
Base pressure	~ 1×10^{-3} Pa
Gas flow / partial pressure of Argon	~70 sccm / ~3×10^{-1} Pa
Flow / partial pressure of N_2 (AlN_x)	≤ 45 sccm / ≤ 3.2×10^{-1} Pa
Flow / partial pressure of O_2 (AlO_y)	≤ 9 sccm / ≤ 7×10^{-2} Pa
Flow / partial pressure of N_2+O_2 (AlN_xO_y)	≤ 27.5 sccm / ≤ 2.2×10^{-1} Pa
Direct Current (DC) applied to the target	75 $A.m^{-2}$
Substrate (glass and silicon) polarization	GND
Substrate holder rotation	9 r.p.m.
Distance between target and substrate holder	~70 mm
Type-K thermocouple temperature	~100 ºC

Table 1. Sputtering conditions/parameters used to produce AlN_x, AlO_y and AlN_xO_y films.

The discharge parameters: target potential and current, gas pressure, argon flow and reactive gas flow, were monitored before and/or during the deposition using an Agilent 34970A Data Acquisition system.

The atomic composition of the samples was measured by Rutherford Backscattering Spectrometry (RBS), in silicon substrates, using 1.4 and 1.75 MeV proton beams and a 2 MeV ^4He beam. Three different detectors were used at scattering angles of 140º and 165º (two detectors, at symmetrical positions with respect to the beam), and experiments were made at tilt angles of 0º and 30º. Composition profiles for the as-deposited samples were determined using the NDF software [48-50].

The deposition rate, or growth rate, was calculated by the ratio between the average thickness of the sample, deposited on silicon substrate, and the deposition time. Scanning electron microscopy (SEM) was used to determine the thickness of the films and to investigate their morphology, using a Leica Cambridge 5526 apparatus.

The structure and phase distribution of the coatings deposited in silicon substrates, were accessed by X-ray diffraction (XRD), using a conventional Philips PW 1710 diffractometer, operating with Cu Kα radiation, in a Bragg–Brentano configuration.

Cross-sectional samples were thinned down to 10 μm by using the tripod polisher. The electron transparency was achieved by ion milling. Conventional and high resolution transmission electron microscopy (TEM) observations were performed on a JEOL 2200-FS microscope (Schottky-FEG, 200 kV) fitted with an omega filter.

The coatings reflectivity and transmission coefficients were measured in glass substrates between 250 nm and 2500 nm using a Shimadzu UV-3101 PC UV-Vis-NIR with an attached integrating sphere of 60 mm (inner diameter). With the purpose of eliminate experimental artifacts caused by the integrating sphere, two standards: a STAN-SSH High-Reflectivity Specular Reflectance Standard (from Ocean Optics) and a WS-1-SL Spectralon White Reflectance Standard (from Labsphere), were used for reflectance measurement correction purposes.

3. RESULTS AND DISCUSSION

3.1 Chemical composition and deposition rates

Figure 1 shows the atomic ratio of non-metallic over aluminium elements (non-metallic/Al) of the three film systems, AlN_x, AlO_y and AlN_xO_y, as a function of the partial pressure of reactive gas. According to the results obtained by RBS analysis, the films composition is uniform across the film thickness within the penetration depth of the beam. As can be seen, when preparing the AlN_x system, there is a smooth and almost linear increase of the nitrogen content in the films as the N_2 partial pressure is increased, until a close-stoichiometric AlN compound is formed for partial pressures higher than 8×10^{-2} Pa. This gradual increase of the N/Al atomic ratio in the films induces differences in the type of atomic bonds formed, changing the films structure and morphology and thus a wide and gradual variation of the optical properties of the resulting compounds. Figure 1 shows also that the evolution of the O/Al atomic ratio in the AlO_y system is not as smooth as that of the AlN_x system, as it can be concluded from the early formation of the close-stoichiometric Al_2O_3 films, for pressures above 4.2×10^{-2} Pa. In fact, one can observe a sudden jump in the O/Al atomic ratio from 0.59 to 1.6 (close-stoichiometric Al_2O_3), by changing the pressure of O_2 from 3.6×10^{-2} Pa to 4.2×10^{-2} Pa.

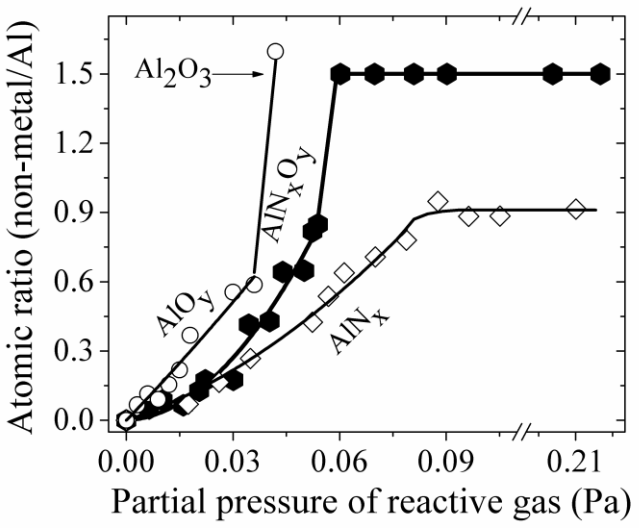

Figure 1. Atomic ratios of the non-metallic/Al elements concentration in the films as a function of the partial pressure of the reactive gas. In the AlO_y system the reactive gas used was pure O_2, in AlN_x films pure N_2, and in the ternary system AlN_xO_y a mixture of N_2+O_2 (17:3) was used. The chemical composition of the coatings was determined by RBS with a resolution of about 3-5 at.% in the elemental concentration.

Regarding the evolution of the ternary oxynitride system, AlN_xO_y, contrarily to what was observed in the binary AlO_y films, one can report a smooth increase of the non-metallic/Al atomic ratio for reactive gas mixture partial pressures up to 5.4×10^{-2} Pa, corresponding to the formation of thin films with (N+O)/Al atomic ratios up to 0.85. For partial pressures of the reactive gas mixture above 5.6×10^{-2} Pa, the nitrogen element is not detected in the films using RBS technique and thus *quasi*-stoichiometric Al_2O_3 films are expected. A similar behaviour was also observed for the zirconium oxynitride films (ZrN_xO_y) prepared using the same deposition system, due to the much higher reactivity of oxygen and the prevalence of the thermodynamic constrains over the kinetic ones [19].

A closer look to the evolution of the x coefficient (N/Al ratio) and y coefficient (O/Al ratio) for both binary systems as well as for the ternary system can be observed in figure 2(a-b). The two figures show the evolution of both x and y individually as a function of the correspondent reactive gas partial pressures. The range of partial pressures goes up to 4.6×10^{-2} Pa for N_2 and 0.8×10^{-2} Pa for O_2, corresponding to 85% and 15% of the maximum reactive mixture (N_2+O_2) partial pressure used to produce AlN_xO_y films. The shaded regions correspond to the pressure values used to produce Al_2O_3 films with the reactive mixture.

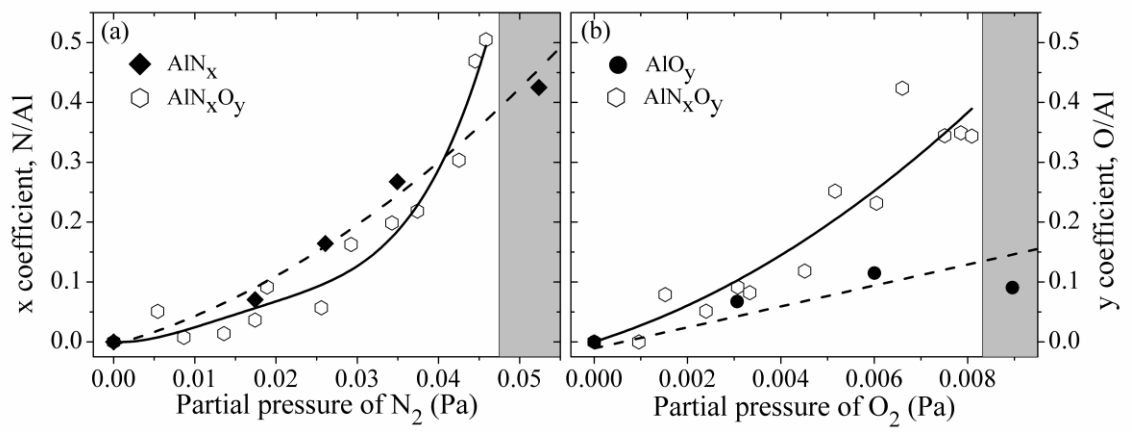

Figure 2. Comparison between the binary and ternary systems concerning their (a) x coefficient and (b) y coefficient. The range of partial pressures of N_2 and O_2 plotted correspond to the fraction of both gases in the reactive mixture, *i.e.* 85% of N_2 and 15% of O_2. The shaded regions correspond to experimental conditions that gave rise to the preparation of Al_2O_3-type films using the reactive mixture (N_2+O_2).

According to figure 2(a) one can observe that for the same partial pressure of N_2, the atomic ratios N/Al in the AlN_xO_y films are close to the ones detected in the AlN_x system. This is, in fact, an expected behaviour since both film systems are produced in N_2 rich reactive atmospheres. In the AlN_xO_y films, beyond the nitride compound formation, the available aluminium atoms can also bond with oxygen to form oxides, due to the higher affinity of aluminium to bond oxygen in comparison with nitrogen [12], resulting in very similar O/Al and N/Al atomic ratios.

On the other hand, figure 2(b) shows that for the same partial pressure of O_2, the atomic ratio O/Al is relatively higher in the AlN_xO_y films when compared to the one observed in the AlO_y system, increasing further the difference as the O_2 partial pressure increases. The main reason for this particular behaviour might be closely related with the target poisoning effect [12, 47]. In the case of AlN_xO_y, the large amount of nitrogen present in the chamber is partially poisoning the aluminium target thus reducing the aluminium sputtering rate and resulting in high O/Al atomic ratio. On the other hand, in the AlO_y system, for the same partial pressure of O_2, the target is in a clean state mode and thus the aluminium sputtering rate is higher than in the AlN_xO_y system. The amount of aluminium atoms arriving at the substrate and available to form oxide compounds is thus very high, resulting in lower O/Al atomic ratios in the AlO_y system. This also explains why the O_2 partial pressure to prepare close-stoichiometric alumina films (O/Al ~ 1.6) is much higher in the AlO_y system, about 4×10^{-2} Pa, than in the ternary system, where the Al_2O_3 films start to form for partial pressures above 0.9×10^{-2} Pa. These features are reinforced by the AlO_y films deposition rates (determined by thickness over deposition time) which were found to be ~40% higher than the ones obtained in AlN_x and AlN_xO_y [47] systems. The values of deposition rates, as well as the thicknesses of some representative films of each system, are presented in table 2.

AlN_x samples	Thickness (µm)	Deposition rate ($nm.min.^{-1}$)	AlO_y samples	Thickness (µm)	Deposition rate ($nm.min.^{-1}$)	AlN_xO_y samples	Thickness (µm)	Deposition rate ($nm.min.^{-1}$)
Al	3.3	37	Al	3.3	37	Al	3.3	37
$AlN_{0.07}$	2.3	39	$AlO_{0.07}$	3.5	59	$AlN_{0.01}O_{0.08}$	3.1	34
$AlN_{0.16}$	2.8	47	$AlO_{0.11}$	3.0	50	$AlN_{0.04}O_{0.09}$	3.2	36
$AlN_{0.27}$	2.4	39	$AlO_{0.15}$	4.5	50	$AlN_{0.09}O_{0.08}$	2.8	46
$AlN_{0.42}$	2.0	22	$AlO_{0.22}$	5.5	61	$AlN_{0.16}O_{0.25}$	2.8	48
$AlN_{0.64}$	1.1	13	$AlO_{0.37}$	5.5	62	$AlN_{0.30}O_{0.34}$	3.4	29
$AlN_{0.71}$	1.3	14	$AlO_{0.56}$	6.0	66	$AlN_{0.51}O_{0.34}$	2.9	24
$AlN_{0.78}$	1.1	12	$AlO_{0.59}$	4.7	52	Al_2O_3	0.2	5
$AlN_{0.88}$	0.7	9	$Al_2O_{3.2}$	0.2	2			
$AlN_{0.91}$	0.8	6						

Table 2. Thickness and deposition rate of the samples, estimated based in cross-section SEM observations.

3.2 Crystalline Structure

In order to follow the influence of the chemical composition in the structural features of the films, a detailed structural characterization was carried out. Figure 3(a-c) shows the XRD diffractograms of the prepared samples, where the differences in crystalline phase formation and preferential growth can be observed. Following the distinct compositions, the structural analysis brings other insights, not only confirming previous identified zones, but also uncovering the development of other important features that will be used to explain the different optical behaviours.

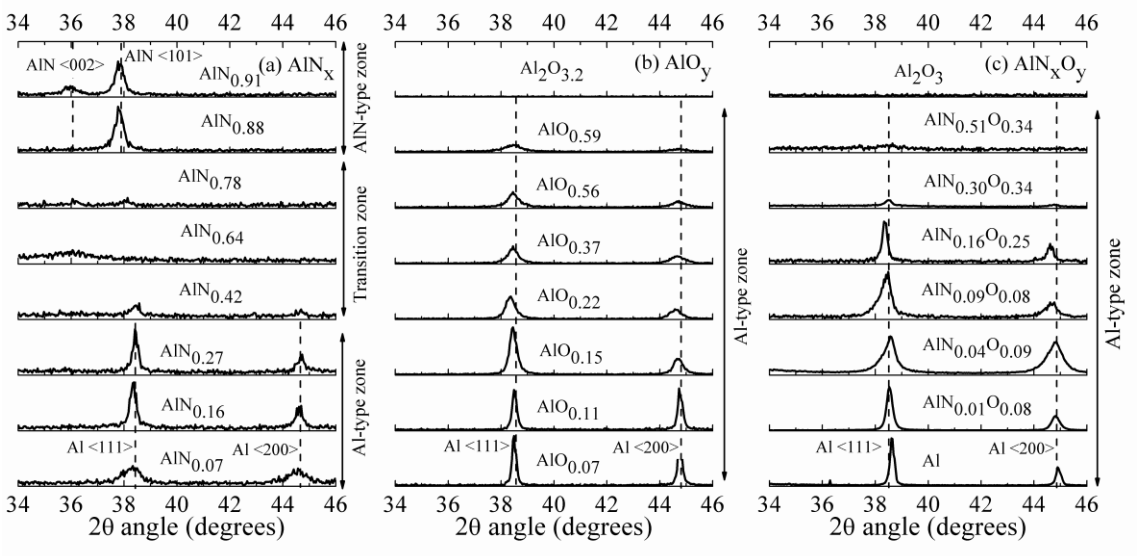

Figure 3. X-ray diffractograms of the (a) AlN_x system, (b) AlO_y system and (c) AlN_xO_y system.

The aluminium film (deposited without reactive gas) exhibits the typical face-centered cubic (fcc) structure of aluminium (ICSD collection code: 52255) [51], with the main diffraction peaks corresponding to <111> and <200> diffraction planes, as can be seen in figure 3(c).

In the previous section it was shown that there are two main behaviours in the AlN_x system. However, according to the XRD measurements depicted in figure 3(a), one can actually distinguish three different zones. The results obtained show an Al-type crystalline structure, followed by a gradual transition towards AlN-type diffraction patterns. The fcc structure of aluminium is clearly observed for atomic ratios N/Al up to x = 0.27 (Al-type zone), which in fact is in agreement with previous investigations carried out by Venkataraj and co-workers [25]. In the films with higher x values (transition zone), the Al-type diffraction peaks seems to vanish, giving rise to faint (low intensity) AlN peaks, as deduced from XRD measurements, namely those with x values between 0.42 and 0.78. Again, this behaviour is closely related with that observed by Venkataraj *et al.* [25]. When the atomic ratio N/Al increases further (AlN-type zone), the films crystallize in a typical hexagonal AlN *wurzite*-type structure (ICSD collection code: 82790), with a <101> preferential orientation, as already demonstrated by other authors using reactive DC magnetron sputtering [25, 52, 53]. The diffraction angle corresponding to the <101> diffraction plane was detected at $2\theta = 38^{\circ}$, which is rather close to the stress-free lattice of the AlN structure ($2\theta = 38.3^{\circ}$). The <002> plane, corresponding to the c-axis orientation of the hexagonal lattice could also be detected in sample $AlN_{0.91}$ at $2\theta = 36^{\circ}$, also in agreement with the $2\theta = 36.3^{\circ}$ value of the stress-free lattice of the AlN hexagonal structure.

In the case of AlO_y system, one can also establish a close relation between the chemical composition and the crystalline structure evolution. The corresponding XRD patterns are plotted in figure 3(b). This figure shows that for atomic ratios O/Al up to y = 0.59, the films crystallize in a fcc Al-type structure, very similar to what was observed in the AlN_x system, but for relatively lower non-metallic/aluminium ratios (N/Al). Furthermore, and in spite of the similarities with the AlN_x system evolution, the Al-type structure found in the sub-stoichiometric AlO_y films, figure 3(b), is not as common as the one observed in the AlN_x system [37, 53, 54]. For example, previous investigations about this system developed by Koski *et al.* [30, 54] reported amorphous films with O/Al atomic ratios close to stoichiometric Al_2O_3 (between 1.3 and 1.7), even if deposited with low O_2 flows. More recently, Drüsedau and co-workers [53] found similar results to those reported by Koski *et al.* which used similar deposition parameters but with a higher substrate temperature (~ 540 K). On the other hand, Cremer *et al.* [55] found a mixture of crystalline aluminium and γ-Al_2O_3, in AlO_y films deposited with low O_2 flow, using also DC magnetron sputtering, however with a higher substrate temperature (~ 798 K).

Still in the AlO_y system, and in agreement with the mentioned studies of Koski *et al.* and Drüsedau *et al.*, one can report that the close-stoichiometric Al_2O_3 films, deposited with higher O_2 partial pressures (above 4.2×10^{-2} Pa), are amorphous, as can be seen in figure 3(b). This feature is to

be expected since the films are formed in relatively low mobility conditions (low temperatures and grounded substrates) and thus the adatoms have limited energy to form Al_2O_3 crystalline-type structure.

Regarding the AlN_xO_y system, and in agreement with the results obtained in the case of the binary systems AlN_x and AlO_y, one can also observe the development of Al-type patterns. In fact, the <111> and <200> planes of the fcc Al-type structure can be found for atomic ratios (N+O)/Al up to 0.41. Then, an increase of the oxygen and nitrogen content induce the formation of films that gradually become amorphous. The close-stoichiometric Al_2O_3 films revealed XRD patterns characteristic of amorphous structures, as it can be evidenced by the diffractogram corresponding to the film with an atomic ratio of 1.5, figure 3(c).

An important feature about the Al-type crystalline structure detected in the three systems is that no significant peak shifting can be observed with the increase of the non-metallic/Al atomic ratios. This could be a sign of limited incorporation of non-metallic elements in the Al lattice, opening the possibility of the existence of pure aluminium particles in the films, even in those with relatively high atomic ratios. In fact, the position of the peaks detected by XRD was found to be approximately the same for x values of up to 0.27 in the AlN_x system, and of up to x = 0.16 in AlN_xO_y. Above these x values, the diffraction peaks are clearly vanishing as can be observed in figure 3(a) and (c). This loss of crystallinity that occurred for lower x values in the AlN_xO_y, is most probably related to the presence of oxygen in the films, since the increase of this element can completely cover the surface of the growing crystals, inhibiting their growth [12, 56]. On the other hand, in the AlO_y system the Al-type structure was obtained for O/Al atomic ratios of up to 0.59, higher than the value y = 0.25 obtained for the AlN_xO_y crystalline samples. This indicates that nitrogen also plays an important role in inhibiting the coarsening of the Al crystals. Further detailed analysis of the structural features, can be found elsewhere [12].

3.3. Optical properties

3.3.1 Reflectance and Transmittance measurements. Since the optical properties of the materials significantly rely on their composition and type of bonding, structure, and morphology, an understanding of these dependencies is of fundamental importance. The changes observed in films chemical composition and structural features are likely to induce significant changes in their optical responses. Figure 4(a-c) shows the absolute reflectance of the opaque samples and figure 5(a-b) the transmittance and reflectance of the semi-transparent ones, for the three systems studied (AlN_x, AlO_y and AlN_xO_y,) in the range of 290 nm to 2500 nm.

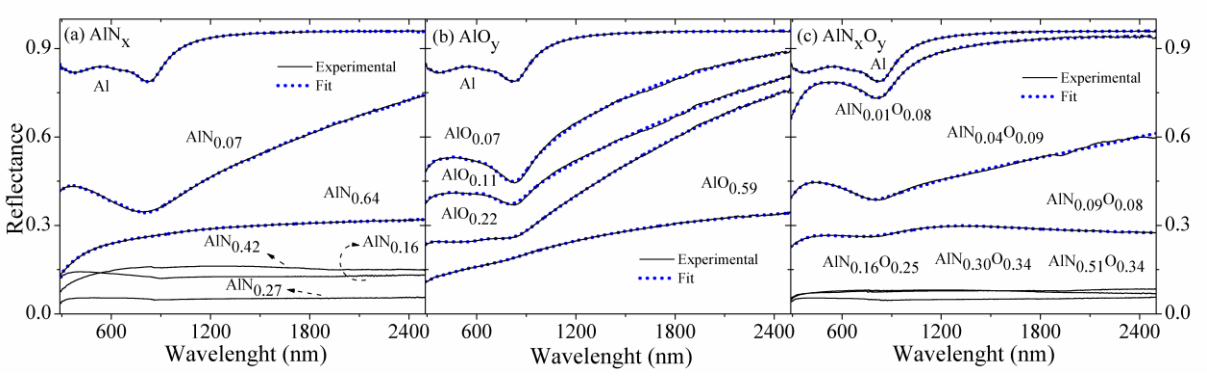

Figure 4. Experimental and fitted reflectance of the opaque samples ascribed to the (a) AlN_x system, (b) AlO_y system and (c) AlN_xO_y system.

The reflectance of the sample deposited without reactive gas has the typical profile of polycrystalline aluminium, with high reflectance values and a strong absorption peak around 800 nm (~ 1.5 eV) due to interband transitions [57]. As the non-metallic/Al atomic ratio increases, the reflectance spectrum of the samples has a pronounced variation, both in form and intensity. This happens regardless of the system in question, changing from a profile with high reflectance values towards a nearly constant spectrum, with relatively low reflectance values for some critical atomic ratios. Concerning the AlN_x system, shown in figure 4(a), the minimum of the reflectance spectrum drops from a value of approximately 78%, for the aluminium sample, to 35% for an atomic ratio N/Al of 0.07. For an atomic ratio of 0.27, the typical interband transition of aluminium at ~ 800 nm is no longer observed and the profile becomes almost flat over the entire measured spectrum, with reflectance reaching values as low as 5%.

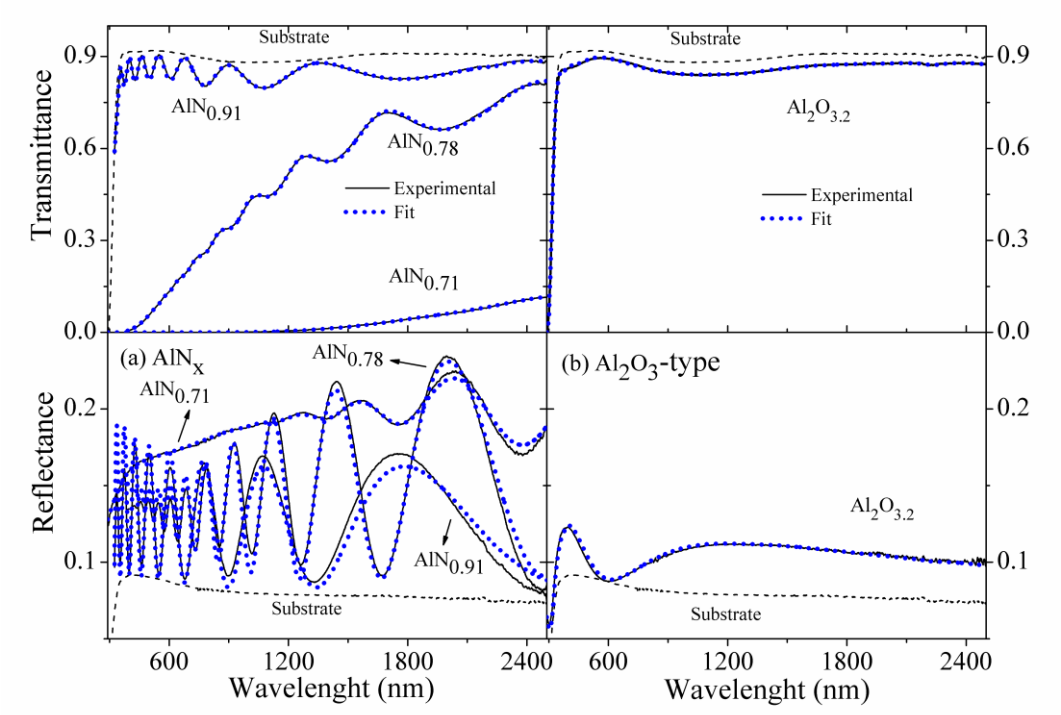

Figure 5 – Experimental and fitted transmittance and reflectance of the semi-transparent samples of the (a) AlN_x system and (b) an Al_2O_3-type sample indexed to the AlO_y system.

Further increasing the atomic ratio the reflectance increases again, with the films becoming semi-transparent for atomic ratios N/Al above 0.71, as one can conclude from figure 5(a), by the appearance of interference fringes for wavelengths higher than 1200 nm in the reflectance spectrum and increasing transmittances values. For an atomic ratio of 0.91, a crystalline hexagonal AlN-type structure is formed and the transmittance of the films reaches its highest value, close to that of the substrate.

In the case of the AlO_y system, figure 4(b), one can observe a gradual decrease of the reflectance as the O/Al atomic ratio increases, with reflectance attaining its minimum for an O/Al ratio of 0.59. Further increasing the oxygen content, the O/Al atomic ratio raised to 1.6 corresponding to a close-stoichiometric alumina film ($Al_2O_{3.2}$), revealing a very high transparency over the measured range of wavelengths, figure 5(b).

In what concerns the optical behaviour of the AlN_xO_y system, figure 4(c), it exhibits a similar trend to that initially observed for the AlN_x system. As the ratio of non-metallic over metallic elements increases, a gradual decrease of the reflectance can be observed, with the interband transition (~ 800 nm) being evident in samples for atomic ratios (N+O)/Al up to 0.17, which is related with the high content of aluminium in the films. For (N+O)/Al atomic ratios between 0.17 and 0.85, the reflectance profile becomes almost flat in the entire measured spectral range, reaching values as low as 5%, similar to what was observed in AlN_x system, but for a wider range of atomic ratios. Important to notice is that the type of growth of the AlN_xO_y films changes from columnar to cauliflower-like, as

discussed elsewhere [12]. In fact, the microstructure analysis of the films with (N+O)/Al atomic ratios between 0.17 and 0.85 revealed that these films present porosities significantly higher than those observed for the films with (N+O)/Al atomic ratios below 0.17. The unusual (cauliflower) type of growth observed for those films induced roughness values as high as 350 nm, which are significantly higher than the ones found for the metallic-like films, which was only about 150 nm (estimated from AFM) [12]. Furthermore, the particular experimental conditions used to prepare AlN_xO_y films with (N+O)/Al ratios between 0.17 and 0.85 resulted in the growth of nanocomposite films, consisting of Al nanoparticles embedded in an amorphous aluminium oxide/nitride or oxynitride matrix, as demonstrated by the DF-TEM micrograph, figure 6(a), and the corresponding diffraction pattern (upper insert, figure 6(b)), as well as the HRTEM in figure 6(c). This type of morphology also explains the electrical properties of the films, as already discussed in a previous work [47]. The lower reflectance values, extending to the near-infrared, that were observed for these nanocomposite films could be due to the formation of a complex shape network of Al nanoparticles in the matrix, since it is known that metallic fractal cluster networks can induce a broadband optical absorption [58]. This is an important optical behaviour, with some possible applications, namely in concentrated solar power systems (CSP), where a material with very low spectral reflectance is required in the range of solar spectrum [59, 60]; as well as in solar collectors [61] and sensors. Finally, for (N+O)/Al atomic ratios above 0.85, the films correspond to quasi-stoichiometric Al_2O_3, presenting a relatively smooth surface morphology (RMS roughness ~3 nm), resulting in transmittance and reflectance spectra very similar to those of figure 5(b).

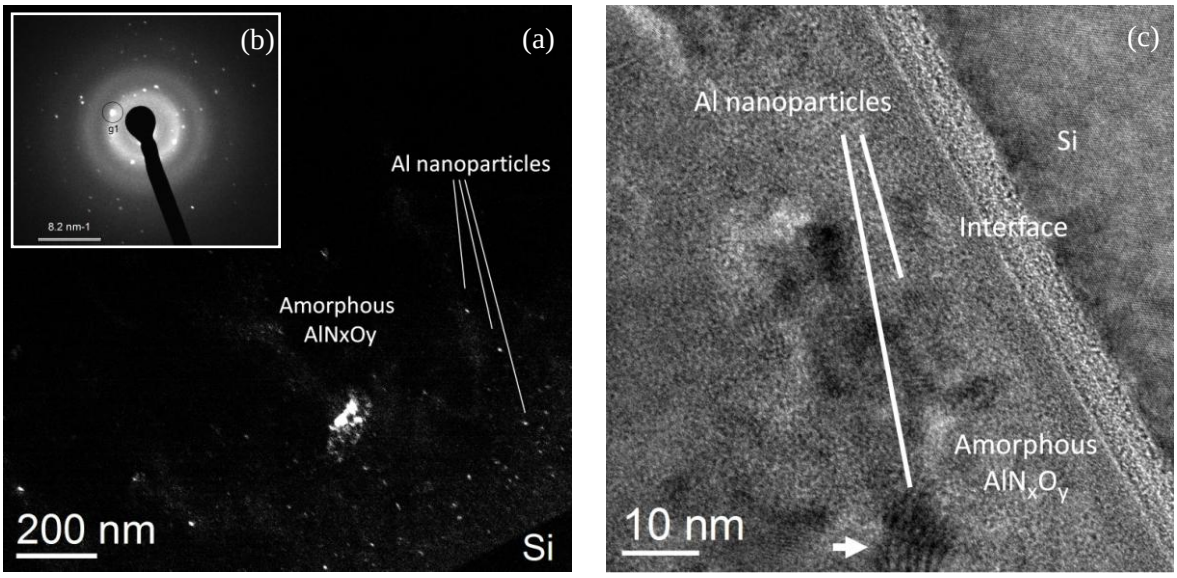

Figure 6 - (a) Cross-sectional Dark-Field TEM micrograph obtained by selecting a spot given by one set of <200> aluminum reflecting planes in Al, which have interplanar distance of 0.215 ± 0.005 nm, showing the distributions of aluminum nanoparticles. The selected area electron diffraction pattern shown in (b) was obtained by probing a circular area of 1 μm diameter in the film. Intense spots, indicating crystalline phases, and faint large rings, revealing amorphous phases, were observed. The circled bright spot labeled g1 in (b) was selected to

form the dark-field image (a). (c) Cross-sectional High Resolution TEM micrograph showing aluminum nanoparticles embedded within the amorphous oxynitride film close to the interface. Some nanoparticles exhibit Moiré contrast (see arrow at the bottom of the micrograph).

3.3.2. Modelling of the optical spectra.

3.3.2.1. Theoretical background. To investigate the optical properties of the films, different optical models were used to fit its reflectance and/or transmittance spectra, using the computer program 'SCOUT' (developed by W. Theiss, Hard- and software) [62]. To describe the dielectric susceptibility of polycrystalline aluminium there are normally three contributions that must be taken into account:

i) The free electron contribution due to intraband transitions, described by a Drude model, which is given by:

$$\chi_{\text{Drude}} = \frac{\Omega_{\text{plasma}}^2}{\tilde{\nu} + i\tilde{\nu}\,\Omega_T} \tag{1}$$

In the equation (1), $\tilde{\nu}$ is the wavenumber, and Ω_{plasma} and Ω_T are the plasma frequency and damping constant, respectively, which are two adjustable parameters of the model.

ii) The interband transition contribution due to two strong interband transitions at 0.5 eV and 1.5 eV. The typical strong absorption band of aluminium, around 800 nm, was described using a OJL interband transition model with the correspondent expressions deduced elsewhere [63].

iii) The contribution of the weak broad interband absorption [26, 28, 57], modelled using two Kim oscillators [64], which is just an extension of the classical harmonic oscillator model that allows a shift of the line shape between a Gaussian and a Lorentzian profile. The susceptibility (χ_{Kim}) is given by:

$$\chi_{\text{Kim}} = \frac{\Omega_P^2}{\Omega_{TO}^2 - \tilde{\nu}^2 - i\tilde{\nu}\tau(\tilde{\nu})}\ ;\ \tau(\tilde{\nu}) = \Omega_\tau \exp\left[-\frac{1}{1+\sigma^2}\left(\frac{\tilde{\nu}-\Omega_{TO}}{\Omega_\tau}\right)^2\right] \tag{2}$$

There are four adjustable parameters in the Kim model: resonance frequency (Ω_{TO}), oscillator strength (Ω_P), damping constant (Ω_τ) and the Gauss-Lorentz-switch (σ). When $\sigma = 0$ a Gaussian profile is obtained and when $\sigma > 5$ the Lorentzian line shape is gained.

The model described above with a dielectric background contribution was used to study the optical properties of the films with Al-type structure in the three systems, considering a simple layer surrounded by air to represent the coating.

Several models can be used to study AlN optical properties such as the Swanepoel´s method [27], the OJL oscillator model, or simply using a two oscillators model [28]: one Brendel [65] and one Kim. The Brendel oscillator model is similar to the Kim oscillator model, with the same four adjustable parameters where the parameter σ is substituted by the distribution width parameter. This two oscillators model (Brendel + Kim) was used to simulate both reflectance and transmittance spectra of the AlN_x films with concentration ratios above 0.88, corresponding to the close-stoichiometric AlN films, as well as for some of the AlN_x films, indexed to the transition zone with a Tauc-Lorentz dielectric function model added. In this model, the imaginary part of the susceptibility χ_i is given by [66, 67]:

$$\chi_i(\omega) = \frac{1}{\omega} \frac{S^2 \omega_0 \omega_T (\omega - \omega_{gap})^2}{(\omega^2 - \omega_0^2)^2 + \omega^2 \omega_T^2} \Theta(\omega - \omega_{gap}) \quad (3)$$

The adjustable parameters are S, strength, ω_T, damping constant, ω_0, resonance frequency, ω_{gap}, the gap energy, and Θ is the Heaviside step function. The real part of the susceptibility is obtained by Kramers-Kroning relations.

The optical properties of alumina-type films, can be studied using a Tauc-Lorentz model [37, 68], or by the well known and often used Cauchy equations [69], which were adopted in the case of this study. According to this empirical equations, the refractive index, $n(\lambda)$, and extinction coefficient, $k(\lambda)$, can be determined by:

$$n(\lambda) = A_n + \frac{B_n}{\lambda^2} + \frac{C_n}{\lambda^4} + \ldots; \; k(\lambda) = A_k + \frac{B_k}{\lambda^2} + \frac{C_k}{\lambda^4} + \ldots \quad (4)$$

The adjustable parameters are the constants A, B and C, and λ is the wavelength.

In the case of the AlN_x and Al_2O_3-like semi-transparent samples, the optical models were implemented in the 'SCOUT' program assuming a two layer material surrounded by air, constituted by a glass substrate and the deposited film. In these cases, the film thickness could also be extracted from the fits.

3.3.2.2. Determination of the coatings optical constants. Figure 4 (a-c) depicts the representative simulated curves for reflectance of the opaque samples and figure 5(a-b) the representative simulated transmittance and reflectance curves of the semi-transparent ones for the three systems, using the models described previously. The agreement between the simulated and experimental data is very

good. The simulated thickness of the semi-transparent films is in agreement with the values estimated by scanning electron microscopy, as can be observed in Table 3, which gives more confidence to the models used.

Sample	**Simulated thickness** (μm)	**Measured thickness** (μm)
$AlN_{0.71}$	1.4	1.3
$AlN_{0.78}$	1.2	1.1
$AlN_{0.88}$	0.68	0.7
$AlN_{0.91}$	0.74	0.8
$Al_2O_{3.2}$	0.18	0.2

Table 3. Comparison between the simulated thickness and the measured thickness of some semi-transparent samples.

Concerning the films with Al-type structure in the three systems, the standard aluminium optical model gives a good agreement between the experimental and simulated results, figure 4 (a-c). It was possible to estimate a plasma frequency value of about 10.4 eV for the pure aluminium coating, lower than the value of 12.5 eV found in literature [57], which is probably due to the presence of lattice defects and residual doping elements such as oxygen. This also explains the value of 210 meV for the damping parameter in the Drude model, higher than the values found for bulk aluminium (60 - 160 meV) [57]. The typical interband absorption of bulk crystalline aluminium is located at 1.4 eV, close to the 1.5 eV value reported in the literature [70], resulting in the significant drop of reflectance clearly observed in the spectra, figure 4(a-c). This interband absorption, as well as another at 0.5 eV, hidden by the intraband absorption, occurs between the occupied and unoccupied (parallel) conduction bands of aluminium [71, 72]. Two other weak interband absorptions [26], positioned at 2.97 eV and 1.73 eV, were also determined by the model using two Kim oscillators. The DC optical conductivity, $\sigma(0)$, of the aluminium coating was also estimated from the Drude parameters, plasma energy and damping, using the following expression [26]:

$$\sigma(0) = \pi \frac{\Omega_{\text{plasma}}^2}{\Omega_{\text{T}}} \tag{5}$$

A DC optical conductivity of ~ 3×10^{17} s^{-1} was obtained in agreement with the value found in literature for metallic aluminium [26].

As the content of non-metallic over aluminium elements in the film increases, a strong decrease in the plasma frequency is observed. This can be explained by the reduction of the number of free electrons donated by aluminium to the conduction band due to the increasing bonding of aluminium with oxygen and nitrogen. The reduction of the plasma frequency explains the observed reduction of reflectance of the samples, figure 4(a-c), as the ratio of non-metallic over aluminium increases.

Regarding the semi-transparent samples, in the case of the AlN_x system figure 5(a), a bandgap of ~ 2.3 eV was obtained for the $AlN_{0.71}$ sample and ~ 4.3 eV for the $AlN_{0.78}$ sample, both lower than the bandgap estimated for the glass substrate, ~ 4.8 eV. These values were estimated by extrapolating the linear part of the curve $(\alpha h\nu)^2$ *vs.* $h\nu$ [73], where α is the simulated absorption coefficient of the film or glass. The $AlN_{0.91}$ and $Al_2O_{3.2}$ samples have bandgap higher than the glass substrate, and could not be calculated by the model.

The simulated refractive index and corresponding extinction coefficient for some of the samples are plotted in figure 7(a-c), as a function of the wavelength (λ). In these plots one can observe the evolution of n and k for the three systems. As can be seen, these optical constants strongly depend of the chemical composition of the corresponding sample. For the pure aluminium coating the complex refractive index is in agreement with the results obtained by other authors [26, 28]. In what concerns the opaque samples, as the ratio of non-metallic over aluminium elements increases the refraction index and extinction coefficient profiles gradually become smoother, with the typical n peak at ~ 800 nm gradually disappearing and the extinction coefficient decreasing monotonically as a function of the atomic (O+N)/Al ratio. The $AlN_{0.91}$ film also reveals a refractive index of about 1.9, very close to the one obtained by other authors [25, 74] for AlN. Finally, the Al_2O_3-type films, figure 7(b-c), reveal refractive indices of about 1.7 close to the typical value of Al_2O_3 [26, 53].

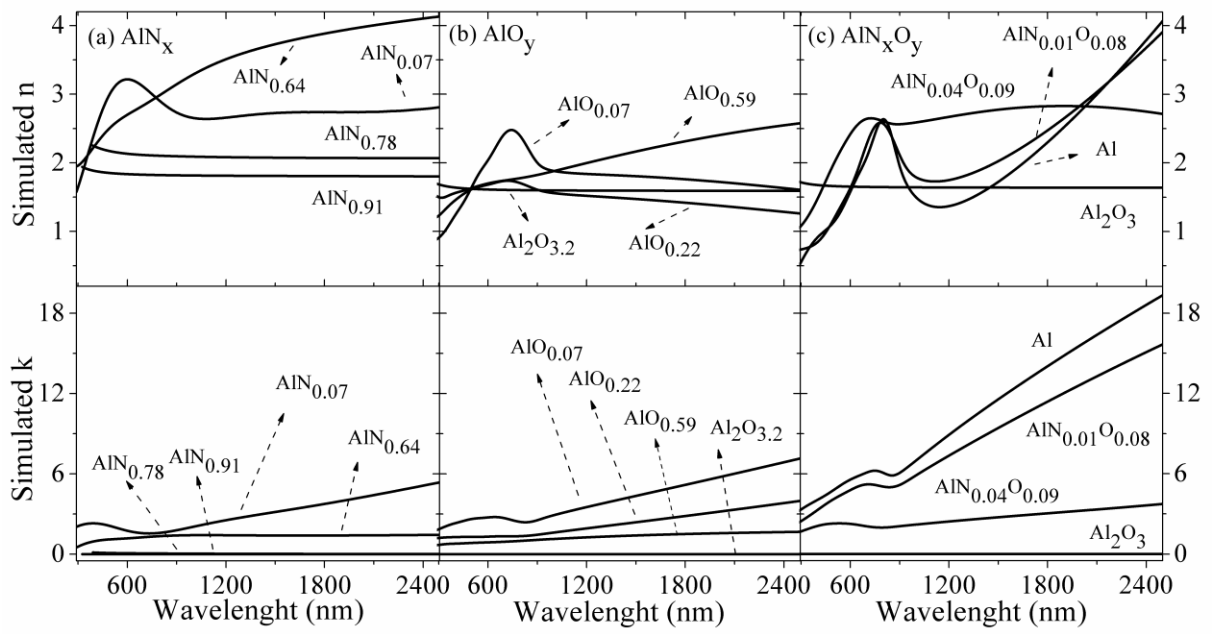

Figure 7. Simulated refractive index and extinction coefficient for some of the samples indexed to the (a) AlN_x system, (b) AlO_y system and (c) AlN_xO_y system.

4. CONCLUSIONS

In order to study whether the ternary system AlN_xO_y has a unique behaviour or is simply a transition between the typical responses of aluminium and of those of the correspondent nitride and oxide, a set of AlN_xO_y films and two sets of the binary systems, AlN_x and AlO_y, were prepared and characterized in detail in terms of chemical composition, structure and optical properties.

The thin films were deposited by reactive DC magnetron sputtering, using an aluminium target and argon as working gas. N_2, O_2 and a mixture of $N_2 + O_2$ (17:3) were used as reactive gases to produce AlN_x, AlO_y and AlN_xO_y films, respectively. Varying the pressure of reactive gas, coatings with different chemical compositions and structural features were obtained as well as distinct optical properties.

It was found that the ternary system, AlN_xO_y, has a distinct optical behaviour from the correspondent binary systems, AlN_x and AlO_y. Nevertheless, some similarities can also be found particularly for low non-metallic/Al atomic ratios. In fact, a common feature in the three systems is the Al-type structure observed in the majority of the deposited films. While maintaining this crystalline structure, the reflectance of the films changed from a typical spectrum of pure aluminium towards a flat profile, reaching values as low as 5%, depending on the particular composition of the films. In this particular case, the content of nitrogen plays an important role in the optical properties of the films. While the typical interband absorption of aluminium at ~ 800 nm is always present in the deposited sub-stoichiometric AlO_y films, for some particular N/Al atomic ratios in the AlN_x system, films with very low and nearly constant optical reflectance over the measured spectral range were obtained. For

higher values of N/Al ratio, an AlN-type hexagonal structure can be found in the AlN_x system, with optical responses quite different from the ones observed in the films with Al-type structure, with a gradual increase of film transparency and bandgap, as the N/Al ratio approaches unit. For films deposited using the $N_2 + O_2$ reactive gas mixture, the flat optical reflectance can be found in a wider range of x values because oxygen is also being introduced in the films. The optical properties observed in these films can be explained assuming a network of aluminium nanoparticles embedded in an oxide/nitride matrix, as XRD diffractograms and TEM micrographs suggest. The nanoparticles can coalesce in irregularly formed clusters with different shapes and sizes in the matrix, which is known to induce flat and low reflectance profiles. This unusual low optical reflectance of some films has potential applications in concentrated solar power systems (CSP), solar collectors, sensors, among others.

ACKNOWLEDGEMENTS

This research is sponsored by FEDER funds through the program COMPETE-*Programa Operacional Factores de Competitividade*, by national funds through FCT-*Fundação para a Ciência e a Tecnologia*, under the projects PTDC/CTM-NAN/112574/2009 and PEST-C-FIS/UI607/2011-2012, and Programa Pessoa 2010/2011 – *Cooperação Portugal/França*, Proc.º 441.00, Project *"COLOURCLUSTER"*. The authors acknowledge Professor Luis Rebouta for the help on using the 'SCOUT' software. J. Borges also acknowledges FCT financial support under PhD grant Nº SFRH/BD/47118/2008 (*financiado por POPH – QREN – Tipologia 4.1 – Formação Avançada, comparticipado pelo Fundo Social Europeu e por fundos nacionais do MCTES*).

REFERENCES

[1] Franchy R 2000 *Surface Science Reports* **38** 195-294
[2] Vaz F, Cerqueira P, Rebouta L, Nascimento S M C, Alves E, Goudeau P, Riviere J P, Pischow K and de Rijk J 2004 *Thin Solid Films* **447-448** 449-54
[3] Carvalho P, Vaz F, Rebouta L, Carvalho S, Cunha L, Goudeau P, Riviere J P, Alves E and Cavaleiro A 2005 *Surface and Coatings Technology* **200** 748-52
[4] Erlat A G, Henry B M, Ingram J J, Mountain D B, McGuigan A, Howson R P, Grovenor C R M, Briggs G A D and Tsukahara Y 2001 *Thin Solid Films* **388** 78-86
[5] Mohamed S H, Anders A, Montero I and Galán L 2007 *Journal of Physics and Chemistry of Solids* **68** 2227-32
[6] Kapoor V J, Turi R A, Xu D and Bailey R S 1994 *IEEE Transactions on Components, Packaging, and Manufacturing Technology (Part A)* **17** 367-72
[7] Hallam B, Tjahjono B and Wenham S 2012 *Solar Energy Materials and Solar Cells* **96** 173-9
[8] Futsuhara M, Yoshioka K and Takai O 1998 *Thin Solid Films* **317** 322-5
[9] Chappé J-M, Martin N, Lintymer J, Sthal F, Terwagne G and Takadoum J 2007 *Applied Surface Science* **253** 5312-6
[10] Mohamed S H, Kappertz O, Ngaruiya J M, Niemeier T, Drese R, Detemple R, Wakkad M M and Wuttig M 2004 *Physica Status Solidi (A)* **201** 90-102
[11] Venkataraj S, Severin D, Mohamed S H, Ngaruiya J, Kappertz O and Wuttig M 2006 *Thin Solid Films* **502** 228-34
[12] Borges J, Vaz F and Marques L 2010 *Applied Surface Science* **257** 1478-83
[13] Borges J, Alves E, Vaz F and Marques L 2011 *International Conference on Applications of Optis and Photonics (Braga)* 8001 80010F
[14] Arvinte R, Borges J, Sousa R E, Munteanu D, Barradas N P, Alves E, Vaz F and Marques L 2011 *Applied Surface Science* **257** 9120-4

[15] Mientus R, Grötschel R and Ellmer K 2005 *Surface and Coatings Technology* **200** 341-5
[16] Banakh O, Steinmann P A and Dumitrescu-Buforn L 2006 *Thin Solid Films* **513** 136-41
[17] Parreira N M G, Polcar T, Martin N, Banakh O and Cavaleiro A 2007 *Plasma Processes and Polymers* **4** S69-S75
[18] Mohamed S H and Shaaban E R 2010 *Materials Chemistry and Physics* **121** 249-53
[19] Carvalho P, Chappe J M, Cunha L, Lanceros-Mendez S, Alpuim P, Vaz F, Alves E, Rousselot C, Espinos J P and Gonzalez-Elipe A R 2008 *Journal of Applied Physics* **103** 104907
[20] Carvalho P, Vaz F, Rebouta L, Cunha L, Tavares C J, Moura C, Alves E, Cavaleiro A, Goudeau P, Le Bourhis E, Riviere J P, Pierson J F and Banakh O 2005 *Journal of Applied Physics* **98** 023715-8
[21] Fenker M, Kappl H, Banakh O, Martin N and Pierson J F 2006 *Surface and Coatings Technology* **201** 4152-7
[22] Chappé J M, Carvalho P, Lanceros-Mendez S, Vasilevskiy M I, Vaz F, Machado A V, Fenker M, Kappl H, Parreira N M G, Cavaleiro A and Alves E 2008 *Surface and Coatings Technology* **202** 2363-7
[23] Petitjean C, Grafouté M, Rousselot C and Pierson J F 2008 *Surface and Coatings Technology* **202** 4825-9
[24] Martin N, Banakh O, Santo A M E, Springer S, Sanjinés R, Takadoum J and Lévy F 2001 *Applied Surface Science* **185** 123-33
[25] Venkataraj S, Severin D, Drese R, Koerfer F and Wuttig M 2006 *Thin Solid Films* **502** 235-9
[26] Palik E D 1998 *Handbook of Optical Constants of Solids* (San Diego: Academic Press)
[27] Mortet V, Nesladek M, Haenen K, Morel A, D'Olieslaeger M and Vanecek M 2004 *Diamond and Related Materials* **13** 1120-4
[28] Zhao S and Wäckelgård E 2006 *Solar Energy Materials and Solar Cells* **90** 1861-74
[29] Shih K K and Dove D B 1994 *Journal of Vacuum Science & Technology A: Vacuum, Surfaces, and Films* **12** 321-2
[30] Koski K, Hölsä J and Juliet P 1999 *Thin Solid Films* **339** 240-8
[31] Sproul W D, Graham M E, Wong M S, Lopez S, Li D and Scholl R A 1995 *Journal of Vaccum Science & Technology A: Vaccum, Surfaces and Films* **13** 1188-91
[32] Gryczynski I, Malicka J, Gryczynski Z, Nowaczyk K and Lakowicz J R 2004 *Analytical Chemistry* **76** 4076-81
[33] Akimov Y and Koh W S 2011 *Plasmonics* **6** 155-61
[34] Akimov Y and Koh W 2011 *Plasmonics* **6** 155-61
[35] Taniyasu Y, Kasu M and Makimoto T 2006 *Nature* **441** 325-8
[36] Guo Q X, Yoshitugu M, Tanaka T, Nishio M and Ogawa H 2005 *Thin Solid Films* **483** 16-20
[37] Barshilia H C, Selvakumar N, Vignesh G, Rajam K S and Biswas A 2009 *Solar Energy Materials and Solar Cells* **93** 315-23
[38] Xiong J, Gu H-s, Hu K and Hu M-z *International Journal of Minerals, Metallurgy, and Materials* **17** 98-103
[39] Qi-Chu Z 1998 *Journal of Physics D: Applied Physics* **31** 355
[40] Segda B G, Jacquet M and Besse J P 2001 *Vacuum* **62** 27-38
[41] Hartnett T M, Bernstein S D, Maguire E A and Tustison R W 1998 *Infrared Physics & Technology* **39** 203-11
[42] Corbin N D 1989 *Journal of the European Ceramic Society* **5** 143-54
[43] Pallone A, Demaree J and Adams J 2004 *Nuclear Instruments and Methods in Physics Research Section B: Beam Interactions with Materials and Atoms* **219-220** 755-8
[44] Kamikawa T, Kawaguchi Y, Vaccaro P O, Ito S and Kawanishi H 2009 *Applied Physics Letters* **95** 031106-3
[45] Zhang F, Wang S W, Liu X J, An L Q and Yuan X Y 2009 *Journal of Applied Physics* **105** 093542
[46] Qi-Chu Z, Zhao K, Zhang B C, Wang L F, Shen Z L, Lu D Q, Xie D L and Li B F 1999 *Journal of Vacuum Science & Technology A: Vacuum, Surfaces, and Films* **17** 2885-90
[47] Borges J, Martin N, Barradas N P, Alves E, Eyidi D, Beaufort M F, Riviere J P, Vaz F and Marques L 2012 *Thin Solid Films* **520** 6709-17
[48] Barradas N P, Jeynes C, Homewood K P, Sealy B J and Milosavljevic M 1998 *Nuclear Instruments and Methods in Physics Research Section B: Beam Interactions with Materials and Atoms* **139** 235-8
[49] Barradas N P, Jeynes C and Webb R P 1997 *Applied Physics Letters* **71** 291-3
[50] Barradas N P, Jeynes C and Harry M A 1998 *Nuclear Instruments and Methods in Physics Research Section B: Beam Interactions with Materials and Atoms* **136-138** 1163-7
[51] Downs R T, Bartelmehs K L, Gibbs G V and Boisen M B 1993 *Am. Miner.* **78** 1104-1107
[52] Xu X-H, Wu H-S, Zhang C-J and Jin Z-H 2001 *Thin Solid Films* **388** 62-7
[53] Drüsedau T P, Neubert T and Panckow A N 2003 *Surface and Coatings Technology* **163-164** 164-8
[54] Koski K, Holsa J and Juliet P 1999 *Surface and Coatings Technology* **116-119** 716-20
[55] Cremer R, Witthaut M, Neuschütz D, Erkens G, Leyendecker T and Feldhege M 1999 *Surface and Coatings Technology* **120-121** 213-8
[56] Petrov I, Barna P B, Hultman L and Greene J E 2003 *Journal of Vacuum Science & Technology A: Vacuum, Surfaces, and Films* **21** S117-S28
[57] Smith D Y and Segall B 1986 *Physical Review B* **34** 5191
[58] Shalaev V M 2000 *Nonlinear Optics of Random Media - Fractal Composites and Metal-Dielectric Films* (Berlin: Springer)
[59] Barlev D, Vidu R and Stroeve P 2011 *Solar Energy Materials and Solar Cells* **95** 2703-25
[60] Sergeant N P, Agrawal M and Peumans P 2009 *SPIE Optics and Photonics (San Diego)* 74100C
[61] Granqvist C G 2003 *Advanced Materials* **15** 1789-803
[62] Theiss W 2002 SCOUT, Thin Film Analysis Software (Aachen)
[63] O´Leary S K, Johnson S R and Lim P K 1997 *Journal of Applied Physics* **82** 3334-40
[64] Kim C C, Garland J W, Abad H and Raccah P M 1992 *Physical Review B* **45** 11749-67
[65] Brendel R 1990 *Applied Physics A: Materials Science & Processing* **50** 587-93

[66] Chen H and Shen W Z 2005 *The European Physical Journal B - Condensed Matter and Complex Systems* **43** 503-7
[67] Jellison G E, Merkulov V I, Puretzky A A, Geohegan D B, Eres G, Lowndes D H and Caughman J B 2000 *Thin Solid Films* **377-378** 68-73
[68] Jellison G E and Modine F A 1996 *Applied Physics Letters* **69** 371-3
[69] Dirk Poelman and Philippe Frederic S 2003 *Journal of Physics D: Applied Physics* **36** 1850
[70] Ehrenreich H, Philipp H R and Segall B 1963 *Physical Review* **132** 1918
[71] Harrison W A 1966 *Physical Review* **147** 467
[72] Ashcroft N W and Sturm K 1971 *Physical Review B* **3** 1898
[73] Abeles F 1972 *Optical properties of solids* (Amsterdam: North-Holland Pub. Co.American Elsevier)
[74] Barshilia H C, Deepthi B and Rajam K S 2008 *Thin Solid Films* **516** 4168-74